

Enhanced Charged Higgs Production through W^\pm -Higgs Fusion

Abdesslam Arhrib^{1,2}, Kingman Cheung^{2,3,4}, Jae Sik Lee^{2,5}, and Chih-Ting Lu³

¹ *Département de Mathématiques, Faculté des*

Sciences et Techniques, B.P 416 Tangier, Morocco

² *Physics Division, National Center for Theoretical Sciences, Hsinchu, Taiwan*

³ *Department of Physics, National Tsing Hua University, Hsinchu 300, Taiwan*

⁴ *Division of Quantum Phases and Devices, School of Physics,*

Konkuk University, Seoul 143-701, Republic of Korea

⁵ *Department of Physics, Chonnam National University,*

300 Yongbong-dong, Buk-gu, Gwangju, 500-757, Republic of Korea

(Dated: August 16, 2022)

Abstract

We study the associated production of a charged Higgs boson with a bottom quark and a light quark at the LHC via $pp \rightarrow H^\pm b j$ in the Two Higgs Doublet Models (2HDMs). Using the effective W approximation, we show that there is exact cancellation among various Feynman diagrams in high energy limit. This may imply that the production of charged Higgs can be significantly enhanced in the presence of large mass differences among the neutral Higgs bosons via W^\pm -Higgs fusion in the $pp \rightarrow H^\pm b j$ process. Particularly, we emphasize the potential enhancement due to a light pseudoscalar boson A , which is still allowed by the current data by which we explicitly calculate the allowed regions in $(M_A, \tan \beta)$ plane, and show that the production cross section can be as large as 0.1 pb for large $\tan \beta$. We also show that the transverse momentum distribution of the b quark can potentially distinguish the W^\pm - A fusion diagram from the top diagram. Finally, we point out further enhancement when we go beyond the 2HDMs.

I. INTRODUCTION

A new scalar boson h was discovered in the run I of LHC with $7 \oplus 8$ TeV energies in 2012 [1, 2]. The combined measurement of the mass of the boson performed by the ATLAS and CMS collaborations based on the data from $h \rightarrow \gamma\gamma$ and $h \rightarrow ZZ \rightarrow 4l$ channels is $m_h = 125.09 \pm 0.21$ (stat.) ± 0.11 (syst.) GeV [3]. Furthermore, the measured properties of the new particle are best described by the standard-model (SM) Higgs boson [4, 5].

The mission of the new LHC run at 13 TeV (and later upgraded to 14 TeV) is two folds: the first task is the improvement of the scalar boson mass and scalar boson coupling measurements and the second one would be to find a clear hint of new physics. By performing accurate measurements of the scalar boson couplings to the SM particles would be helpful to determine if the Higgs-like particle is indeed the SM Higgs boson or a Higgs boson that belongs to a higher representation, such as models with extra Higgs doublets, extra triplets, or singlets. Most of higher Higgs representations with extra doublet or triplet Higgs fields predict in their spectrum one or more singly- or doubly-charged Higgs bosons. A discovery of such charged Higgs bosons would be an indisputable signal of new physics.

In the two-Higgs-doublet models (2HDMs) or the minimal supersymmetric standard model (MSSM), the charged Higgs boson can be abundantly produced both at hadron and e^+e^- colliders. At hadron colliders, the charged Higgs boson can be produced through several channels:

- Production from top decay. If the mass of the charged Higgs boson is smaller than $m_t - m_b$, the production of $t\bar{t}$ pairs provides an excellent source of the charged Higgs bosons. If kinematically allowed, one of the top and anti-top quarks, say the anti-top quark can decay into $H^-\bar{b}$, competing with the SM decay decay of $\bar{t} \rightarrow W^-\bar{b}$. This mechanism $pp \rightarrow t\bar{t} \rightarrow t\bar{b}H^-$ can provide an important source of light charged Higgs bosons and offers a much cleaner signature than that of direct production.
- Single charged Higgs production. The most important ones are $gb \rightarrow tH^-$ and $gg \rightarrow t\bar{b}H^-$ [6]. These are QCD processes, and thus the cross sections are expected to be large. We can also have a single charged Higgs boson produced in association with a W^\pm gauge boson via the loop process $gg \rightarrow W^\pm H^\mp$ or the tree level process $b\bar{b} \rightarrow W^\pm H^\mp$ [7]. Similarly, the single charged Higgs boson can be produced in association

with a Higgs boson: $q\bar{q}' \rightarrow W^{\pm*} \rightarrow \phi H^{\pm}$ where ϕ denotes one of the three neutral MSSM Higgs bosons [8]. Most of these processes are of the Drell-Yan type, they are expected to give substantial cross sections only for the charged Higgs mass below about 200 GeV.

- Single charged Higgs boson production associated with a bottom quark and a light quark $qb \rightarrow q'H^+b$ in the MSSM framework in which the neutral heavier Higgs bosons are almost degenerate [9].
- Charged Higgs pair production through $q\bar{q}$ annihilation [10] or gluon fusion.
- Resonant charged Higgs production $c\bar{s} \rightarrow H^+$, $c\bar{b} \rightarrow H^+$ [11].

At the Tevatron and LHC, detection of light charged Higgs boson with $M_{H^{\pm}} < m_t - m_b$ is straightforward from $t\bar{t}$ production followed by the decay $\bar{t} \rightarrow \bar{b}H^-$ or $t \rightarrow bH^+$. Such a light charged Higgs boson can be detected for any value of $\tan\beta$ in the $\tau\nu$ decay which is indeed the dominant decay mode. The ATLAS and CMS have already had an exclusion on $B(t \rightarrow bH^+) \times B(H^{\pm} \rightarrow \tau\nu)$ based on this decay channel [12, 13].

In the MSSM and 2HDMs, the heavy charged Higgs boson with $M_{H^{\pm}} \gtrsim m_t$ would decay predominantly into $t\bar{b}$. The experimental search is rather difficult due to large irreducible and reducible backgrounds associated with $H^+ \rightarrow t\bar{b}$ decay. However, in Refs. [14] it has been demonstrated that the $H^+ \rightarrow t\bar{b}$ signature can lead to a visible signal at the LHC provided that the charged Higgs mass is below 600 GeV and $\tan\beta$ is either below $\lesssim 1.5$ or above $\gtrsim 40$. An alternative decay mode to detect a heavy charged Higgs boson is $H^{\pm} \rightarrow \tau\nu$ [15], even if such a decay is suppressed for heavy charged Higgs bosons, it has the advantage of being much cleaner than $H^+ \rightarrow t\bar{b}$. Recently, a new technique using the jet substructure for the heavy charged Higgs boson decaying to $t\bar{b}$ has been proposed in [16].

In the MSSM, the branching ratio of the decay mode $B(H^{\pm} \rightarrow W^{\pm}h)$ could at best be at the level of 10% for low $\tan\beta$ while in the 2HDM-I * it could dominate over $B(H^+ \rightarrow t\bar{b})$. Therefore, $H^{\pm} \rightarrow W^{\pm}h$ could be an alternative channel to discover the heavy charged Higgs boson at the LHC [17]. Similarly, when the CP-odd Higgs boson A is light enough, the decay of $H^{\pm} \rightarrow W^{\pm}A$ could be the dominant one in the 2HDMs and could also be used to search for heavy charged Higgs bosons. Finally, in the models with higher Higgs representations

* See Section II for classification of 2HDMs.

such as the triplet representation of the Higgs, the charged Higgs boson could decay into $W^\pm Z$ with a significant branching fraction [18]. This decay channel could lead to isolated leptons in the final state and could be used to distinguish between models with charged Higgs bosons.

The aim of this work is to study singly-charged Higgs boson production in association with a bottom quark and a jet q' with the subprocess $qb \rightarrow q'H^+b$. Such a process had been studied for the first time in Ref. [9] which showed that the rate is rather small in the MSSM due to a huge cancellation between the top- and Higgs-mediated diagrams as we will show. In the present study, we discuss the production rate of this process and its sensitivity to $\tan\beta$ in the 2HDMs where the masses of the heavier Higgs bosons are not fixed by one mass parameter as in the MSSM. Specifically, we demonstrate that the process possesses destructive interference between the s - and t -channel diagrams, which significantly reduces the cross section. Especially, when the two heavier neutral Higgs bosons are decoupled from the lightest one and they are degenerate, the cross section is canceled to a large extent. In addition, we show that with a relatively light CP-odd Higgs boson, which is still allowed by the current data, the production cross section of the charged Higgs boson via W^\pm -Higgs fusion in the $pp \rightarrow H^\pm b j$ process can be significantly enhanced at the LHC.

The organization of the work is as follows. In the next section, we write down the framework for the 2HDMs, provide analytic understanding of the process in terms of the $2 \rightarrow 2$ subprocess, and also describe the full $2 \rightarrow 3$ process in detail. We present the numerical results in Sec. III. Some cases beyond the 2HDMs are considered in Sec. IV and we conclude in Sec. V.

II. $qb \rightarrow q'H^+b$ IN TWO HIGGS DOUBLET MODELS

A. Brief review of two-Higgs-doublet models

In 2HDMs the electroweak symmetry breaking is performed by two scalar fields Φ_1 and Φ_2 which are parameterized by [†] :

$$\Phi_1 = \begin{pmatrix} \phi_1^+ \\ \frac{1}{\sqrt{2}}(v_1 + \phi_1^0 + ia_1) \end{pmatrix}; \quad \Phi_2 = e^{i\xi} \begin{pmatrix} \phi_2^+ \\ \frac{1}{\sqrt{2}}(v_2 + \phi_2^0 + ia_2) \end{pmatrix}. \quad (1)$$

[†] For an overview, see Ref. [19].

TABLE I. Classification of 2HDMs satisfying the Glashow-Weinberg condition [22] which guarantees the absence of tree-level FCNC.

	2HDM I	2HDM II	2HDM III	2HDM IV
η_1^d	0	1	0	1
η_2^d	1	0	1	0
η_1^l	0	1	1	0
η_2^l	1	0	0	1

We denote $v_1 = v \cos \beta = v c_\beta$ and $v_2 = v \sin \beta = v s_\beta$. The parameterization of the general scalar potential which is gauge invariant and possesses a general CP structure can be found in [20]. In the present study we are mainly interested in Higgs coupling to fermions and gauge couplings to be listed slightly later.

The general structure for Yukawa couplings is given in the following interactions

$$\begin{aligned}
-\mathcal{L}_Y = & h_u \overline{u_R} Q^T (i\tau_2) \Phi_2 + h_d \overline{d_R} Q^T (i\tau_2) \left(-\eta_1^d \tilde{\Phi}_1 - \eta_2^d \tilde{\Phi}_2 \right) \\
& + h_l \overline{l_R} L^T (i\tau_2) \left(-\eta_1^l \tilde{\Phi}_1 - \eta_2^l \tilde{\Phi}_2 \right) + \text{h.c.}
\end{aligned} \tag{2}$$

where $Q^T = (u_L, d_L)$, $L^T = (\nu_L, l_L)$, and $\tilde{\Phi}_i = i\tau_2 \Phi_i^*$ with

$$i\tau_2 = \begin{pmatrix} 0 & 1 \\ -1 & 0 \end{pmatrix}. \tag{3}$$

We note that there is a freedom to redefine the two linear combinations of Φ_2 and Φ_1 to eliminate the coupling of the up-type quarks to Φ_1 [21]. The 2HDMs are classified according to the values of $\eta_{1,2}^l$ and $\eta_{1,2}^d$ as in Table I.

To define the Higgs mass eigenstates, we first rotate the imaginary components a_i and the charged ones ϕ_1^+ and ϕ_2^+ in order to obtain the would-be-goldstones G^0 and G^\pm that would be eaten by the longitudinal components of the Z and W^\pm bosons. These rotations result in an CP-odd state $a = A = -s_\beta a_1 + c_\beta a_2$ and a pair of charged Higgs bosons $H^\pm = -s_\beta \phi_1^\pm + c_\beta \phi_2^\pm$. In the most general case with CP violation, the mass eigenstates of the neutral Higgs bosons are obtained by diagonalizing the 3×3 mass matrix \mathcal{M}_0^2 by an orthogonal 3×3 mixing matrix O that relates the interaction eigenstates to the mass

eigenstates as follow:

$$(\phi_1^0, \phi_2^0, a)_\alpha^T = O_{\alpha i} (H_1, H_2, H_3)_i^T \quad (4)$$

such that $O^T \mathcal{M}_0^2 O = \text{diag}(M_{H_1}^2, M_{H_2}^2, M_{H_3}^2)$ with the ordering of $M_{H_1} \leq M_{H_2} \leq M_{H_3}$. Here the states H_i do not have to carry any definite CP-parity and they have both CP-even and CP-odd components.

After identifying the Yukawa couplings by

$$h_u = \frac{\sqrt{2}m_u}{v} \frac{1}{s_\beta}; \quad h_d = \frac{\sqrt{2}m_d}{v} \frac{1}{\eta_1^d c_\beta + \eta_2^d s_\beta}; \quad h_l = \frac{\sqrt{2}m_l}{v} \frac{1}{\eta_1^l c_\beta + \eta_2^l s_\beta}, \quad (5)$$

one can easily obtain, from the above Lagrangian, the following Higgs-fermion-fermion interactions

$$\begin{aligned} -\mathcal{L}_{H_i \bar{f} f} = & \frac{m_u}{v} \left[\bar{u} \left(\frac{O_{\phi_2 i}}{s_\beta} - i \frac{c_\beta}{s_\beta} O_{ai} \gamma_5 \right) u \right] H_i \\ & + \frac{m_d}{v} \left[\bar{d} \left(\frac{\eta_1^d O_{\phi_1 i} + \eta_2^d O_{\phi_2 i}}{\eta_1^d c_\beta + \eta_2^d s_\beta} - i \frac{\eta_1^d s_\beta - \eta_2^d c_\beta}{\eta_1^d c_\beta + \eta_2^d s_\beta} O_{ai} \gamma_5 \right) d \right] H_i \\ & + \frac{m_l}{v} \left[\bar{l} \left(\frac{\eta_1^l O_{\phi_1 i} + \eta_2^l O_{\phi_2 i}}{\eta_1^l c_\beta + \eta_2^l s_\beta} - i \frac{\eta_1^l s_\beta - \eta_2^l c_\beta}{\eta_1^l c_\beta + \eta_2^l s_\beta} O_{ai} \gamma_5 \right) l \right] H_i \end{aligned} \quad (6)$$

and

$$\begin{aligned} -\mathcal{L}_{H^\pm \bar{u} d} = & -\frac{\sqrt{2}m_u}{v} \left(\frac{c_\beta}{s_\beta} \right) \bar{u} P_L d H^+ - \frac{\sqrt{2}m_d}{v} \left(\frac{\eta_1^d s_\beta - \eta_2^d c_\beta}{\eta_1^d c_\beta + \eta_2^d s_\beta} \right) \bar{u} P_R d H^+ \\ & - \frac{\sqrt{2}m_l}{v} \left(\frac{\eta_1^l s_\beta - \eta_2^l c_\beta}{\eta_1^l c_\beta + \eta_2^l s_\beta} \right) \bar{\nu} P_R l H^+ + \text{h.c.}, \end{aligned} \quad (7)$$

where $P_{L,R} = (1 \mp \gamma_5)/2$.

Before moving to the next subsection, we present the mixing matrix O in the CP-conserving case in terms of the mixing angle α . In our numerical study, to deliver our findings more clearly, we focus on the CP-conserving case. In this case the matrix O takes the following form:

$$O = \begin{pmatrix} -\sin \alpha & \cos \alpha & 0 \\ \cos \alpha & \sin \alpha & 0 \\ 0 & 0 & 1 \end{pmatrix}, \quad (8)$$

assuming H_3 is the pure CP-odd state or $H_3 = A$. In this notation, the decoupling limit of the 2HDM [23], which seems to be favored by the current LHC data, is $\beta - \alpha \rightarrow \pi/2$:

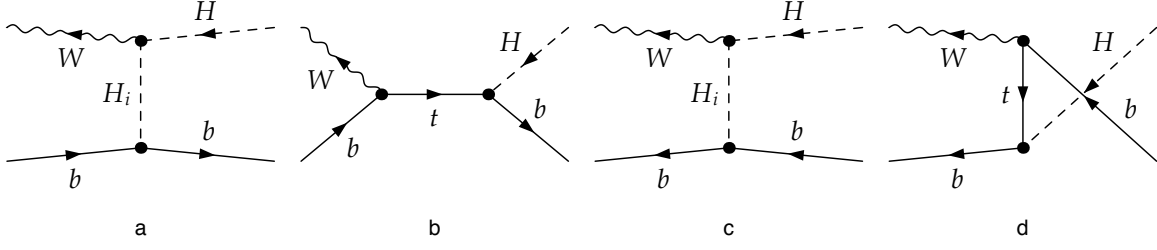


FIG. 1. Feynman diagrams for $2 \rightarrow 2$ subprocesses: $W^+b \rightarrow H^+b$ (a) and (b), $W^+\bar{b} \rightarrow H^+\bar{b}$ (c) and (d).

$$\begin{aligned}
O_{\phi_{11}} &= -\sin \alpha \rightarrow \cos \beta, & O_{\phi_{12}} &= \cos \alpha \rightarrow \sin \beta; \\
O_{\phi_{21}} &= \cos \alpha \rightarrow \sin \beta, & O_{\phi_{22}} &= \sin \alpha \rightarrow -\cos \beta.
\end{aligned} \tag{9}$$

B. Subprocess $W^+b \rightarrow H^+b$ and unitarity

In this subsection, we present the amplitude of the process $qb \rightarrow q'H^\pm b$ in the effective W approximation. In this process, the dominant contribution comes from the region where the W boson emitted from the incoming quark q is close to on shell and one can approximately represent the process by the W boson scattering with the incoming b quark or anti- b quark to give $H^\pm b$ or $H^\pm \bar{b}$ in the final state:

$$\begin{aligned}
W^+(q_1) b(p_1) &\rightarrow H^+(q_2) b(p_2). \\
W^+(q_1) \bar{b}(p_1) &\rightarrow H^+(q_2) \bar{b}(p_2).
\end{aligned} \tag{10}$$

The process $W^+b \rightarrow H^+b$ receives contributions from Fig. 1(a) a t -channel diagram with the neutral H_i exchanges and Fig. 1(b) a s -channel diagram with top exchange. While the process $W^+\bar{b} \rightarrow H^+\bar{b}$ receives contributions from Fig. 1(c) a t -channel diagram with the neutral H_i exchanges and Fig. 1(d) a u -channel diagram with top exchange. The relevant interactions needed for these two subprocesses can be obtained from the Yukawa interactions

given by Eqs. (6) and (7) and from the covariant derivatives:

$$\begin{aligned}
\mathcal{L}_{H_i \bar{b} b} &= -\frac{gm_b}{2m_W} \bar{b} (g_i^S + i g_i^P \gamma_5) b H_i, \\
\mathcal{L}_{H^\pm t b} &= +\frac{gm_b}{\sqrt{2}m_W} \bar{b} (c_L P_L + c_R P_R) t H^\pm + \text{h.c.}, \\
\mathcal{L}_{W^\pm t b} &= -g/\sqrt{2} (\bar{t} \gamma_\mu P_L b) W^{+\mu} + \text{h.c.}, \\
\mathcal{L}_{H_i H^\pm W^\pm} &= -\frac{g}{2} (S_i + i P_i) \left[H^\pm \left(i \overleftrightarrow{\partial}_\mu \right) H_i \right] W^{+\mu} + \text{h.c.}, \tag{11}
\end{aligned}$$

where

$$S_i = c_\beta O_{\phi_2 i} - s_\beta O_{\phi_1 i}, \quad P_i = O_{a i}, \tag{12}$$

and

$$c_L = \tan \beta, \quad c_R = \frac{m_t}{m_b} \frac{1}{\tan \beta}; \quad g_i^S = \frac{O_{\phi_1 i}}{c_\beta}, \quad g_i^P = -\tan \beta O_{a i} \tag{13}$$

in types II and IV and

$$c_L = -\frac{1}{\tan \beta}, \quad c_R = \frac{m_t}{m_b} \frac{1}{\tan \beta}; \quad g_i^S = \frac{O_{\phi_2 i}}{s_\beta}, \quad g_i^P = \frac{O_{a i}}{\tan \beta} \tag{14}$$

in types I and III.

The amplitude of each diagram for $W^+(q_1) b(p_1) \rightarrow H^+(q_2) b(p_2)$ reads

$$\mathcal{M}_{(b)} = -\frac{g^2 m_b C_v}{2m_W(s - m_t^2)} [c_L \bar{u}(p_2) \not{p}_t \not{\epsilon}(q_1) P_L u(p_1) + c_R m_t \bar{u}(p_2) \not{\epsilon}(q_1) P_L u(p_1)], \tag{15}$$

$$\mathcal{M}_{(a)}^{H_i} = -\frac{g^2 m_b}{4m_W(t - M_{H_i}^2)} (S_i + i P_i) (q_2 + p_{H_i})^\mu \epsilon_\mu(q_1) [\bar{u}(p_2) (g_i^S + i g_i^P \gamma_5) u(p_1)],$$

where $s = (p_1 + q_1)^2 = (p_2 + q_2)^2$, $t = (p_1 - p_2)^2 = (q_2 - q_1)^2$, and $u = (p_1 - q_2)^2 = (p_2 - q_1)^2$ and $\epsilon^\mu(q_1)$ denotes the polarization vector of W^+ boson. In the high-energy limit, $s, |t|, |u| \gg m_W^2, m_t^2, M_{H_i}^2, M_{H^\pm}^2$, we find that

$$\begin{aligned}
\mathcal{M} = \mathcal{M}_{(b)} + \sum_i \mathcal{M}_{(a)}^{H_i} &\approx \frac{g^2 m_b}{4m_W^2} \left\{ \left[\sum_i (S_i g_i^S - P_i g_i^P) + i \sum_i (S_i g_i^P + P_i g_i^S) \right] \bar{u}(p_2) P_R u(p_1) \right. \\
&\quad \left. + \left[\left(2c_L + \sum_i (S_i g_i^S + P_i g_i^P) \right) + i \sum_i (-S_i g_i^P + P_i g_i^S) \right] \bar{u}(p_2) P_L u(p_1) \right\}, \tag{16}
\end{aligned}$$

where we have taken the longitudinally polarized W or $\epsilon^\mu(q_1) \approx q_1^\mu/m_W = (p_t^\mu - p_1^\mu)/m_W$ with p_t denoting the four-momenta of the top quark and $p_t^2 = s$. Incidentally, the square of

the 4-momenta of the internal neutral Higgs is $p_{H_i}^2 = (p_1 - p_2)^2 = t$. We note that, in the high-energy limit,

$$\begin{aligned} \overline{|\mathcal{M}|^2} \propto & \left\{ \left| 2c_L + \sum_i (S_i g_i^S + P_i g_i^P) \right|^2 + \left| \sum_i (S_i g_i^S - P_i g_i^P) \right|^2 \right. \\ & \left. + \left| \sum_i (-S_i g_i^P + P_i g_i^S) \right|^2 + \left| \sum_i (S_i g_i^P + P_i g_i^S) \right|^2 \right\} (-t) \end{aligned} \quad (17)$$

and therefore the absence of this unitarity-breaking term requires the following three types of sum rules:

$$\begin{aligned} 2c_L + \sum_i (S_i g_i^S + P_i g_i^P) &= 0, \\ \sum_i S_i g_i^S &= \sum_i P_i g_i^P, \\ \sum_i S_i g_i^P &= \sum_i P_i g_i^S = 0. \end{aligned} \quad (18)$$

The first one gives the relation between the charged Higgs coupling to t and b quarks (c_L) and the sum over the Higgs states of the scalar and pseudoscalar products ($g_i^S S_i + g_i^P P_i$) of the neutral Higgs couplings to b quarks and those to the charged Higgs and W . The second relation shows the sum over the Higgs states of the scalar products should be the same as that of the pseudoscalar ones. And the third relation implies that there is no CP violation if the scalar-pseudoscalar products are summed over the three Higgs states.

These interesting sum rules can be explicitly checked in each 2HDM. In types II and IV, using the orthogonality of the mixing matrix O , we find that

$$\begin{aligned} \sum_i S_i g_i^S &= \sum_i (O_{\phi_2 i} O_{\phi_1 i} - \tan \beta O_{\phi_1 i}^2) = -\tan \beta, \\ \sum_i P_i g_i^P &= -\tan \beta \sum_i O_{ai}^2 = -\tan \beta, \\ \sum_i S_i g_i^P &= \sum_i P_i g_i^S = 0. \end{aligned} \quad (19)$$

With $c_L = \tan \beta$, the unitarity conditions are satisfied automatically. On the other hand, in

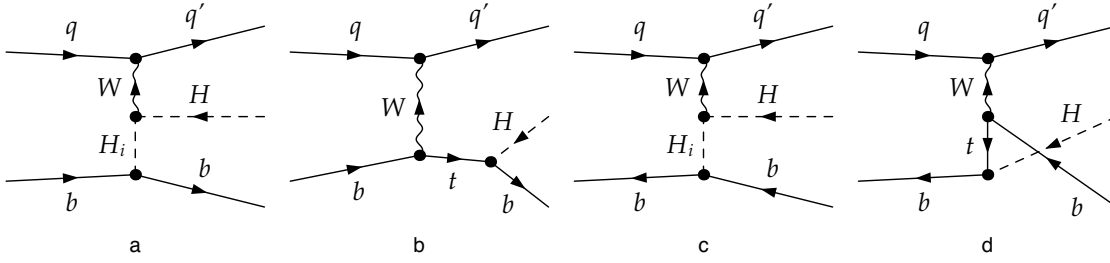


FIG. 2. Feynman diagrams for $qb \rightarrow q'H^+b$ (a) and (b), $q\bar{b} \rightarrow q'H^+\bar{b}$ (c) and (d) where $(q, q') = (u, d), (c, s)$ and $H_i = h, H, A$. The processes with $(\bar{q}, \bar{q}') = (\bar{d}, \bar{u}), (\bar{s}, \bar{c})$ are understood.

types I and III, we find that

$$\begin{aligned}
\sum_i S_i g_i^S &= \sum_i \left(\frac{O_{\phi_2 i}^2}{\tan \beta} - O_{\phi_1 i} O_{\phi_1 i}^2 \right) = 1/\tan \beta, \\
\sum_i P_i g_i^P &= \sum_i \frac{O_{ai}^2}{\tan \beta} = 1/\tan \beta, \\
\sum_i S_i g_i^P &= \sum_i P_i g_i^S = 0.
\end{aligned} \tag{20}$$

With $c_L = -1/\tan \beta$, the unitarity conditions are again satisfied automatically.

This is the proof for the unitarity of the subprocess $W^+b \rightarrow bH^+$ in the high energy limit in the general 2HDMs with or without CP violation. The same proof also applies to the case of \bar{b} initiated subprocess $W^+\bar{b} \rightarrow \bar{b}H^+$.

C. The full process $qb \rightarrow q'H^+b$

After discussing the essence of the physics involved in the $2 \rightarrow 2$ subprocess, we shall describe the full $2 \rightarrow 3$ process. We shall consider the CP-conserving case for simplicity, unless stated otherwise. In this case, without loss of generality, we identify $H_1 = h$, $H_2 = H$, and $H_3 = A$, where h and H denote the lighter and heavier CP-even Higgs bosons, respectively, and A the CP-odd one. The Feynman diagrams for the subprocesses $qb \rightarrow q'H^+b$ and $q\bar{b} \rightarrow q'H^+\bar{b}$ are shown in Fig. 2. We stress at this level one important difference between the bottom-initiated diagram in Fig. 2(b) and anti-bottom-initiated one in Fig. 2(d) is that the former has a s -channel exchange top propagator while the latter has a u -channel one. Similarly, the fermion-line direction of the q can be reversed to include $\bar{q} \rightarrow \bar{q}'$ transition.

TABLE II. The bottom quark Yukawa couplings for h, H, A and that of the charged Higgs boson for 2HDMs of type I, II, III, and IV. The common factor for neutral Higgs boson is $gm_b/\sqrt{2}M_W$ while that for the charged Higgs is $g/\sqrt{2}M_W$. The chiral projection operators are $P_{L,R} = (1 \mp \gamma^5)/2$.

	Type I, III	Type II, IV
$hb\bar{b}$	$\frac{\cos \alpha}{\sin \beta}$	$-\frac{\sin \alpha}{\cos \beta}$
$Hb\bar{b}$	$\frac{\sin \alpha}{\sin \beta}$	$\frac{\cos \alpha}{\cos \beta}$
$Ab\bar{b}$	$+\cot \beta$	$-\tan \beta$
$H^- t\bar{b}$	$-\frac{m_b}{\tan \beta} P_L + \frac{m_t}{\tan \beta} P_R$	$m_b \tan \beta P_L + \frac{m_t}{\tan \beta} P_R$

Therefore, we have a number of initial states for production of H^+ : $(u, c, \bar{d}, \bar{s}) \otimes (b, \bar{b})$. We can then take the charge conjugate to obtain the H^- processes.

The diagram in Fig. 2(b) represents a top-induced process. If $M_{H^\pm} < m_t - m_b$, the top quark is produced on-shell, then followed by its decay into bH^+ . This diagram is entirely dominant over the other diagrams. However, when $M_{H^\pm} > m_t - m_b$ the top quark is off-shell, and thus other diagrams also make significant contributions. In other diagrams, the charged Higgs boson appears being produced by WH_i fusion, where $H_i = h, H, A$ in the CP-conserving case. The coupling in the vertex $W^+ H^- H_i$ is a gauge coupling proportional to g and some mixing angles of the Higgs sector, and independent of different types of 2HDMs. On the other hand, the dependence on the type of 2HDMs comes from the Yukawa couplings of H_i to b quark and the charged Higgs boson to tb . We list the relevant Yukawa couplings for 2HDMs from type I to IV in Table II up to some normalizations. Incidentally, the non-vanishing neutral Higgs couplings to charged Higgs and W are given by

$$\begin{aligned}
S_1 = S_h &= c_\beta O_{\phi_{21}} - s_\beta O_{\phi_{11}} = \cos(\beta - \alpha), \\
S_2 = S_H &= c_\beta O_{\phi_{22}} - s_\beta O_{\phi_{12}} = -\sin(\beta - \alpha), \\
P_3 = P_A &= O_{a3} = 1,
\end{aligned} \tag{21}$$

using the form of O given by Eq. (8).

In the decoupling limit, we have $\cos(\beta - \alpha) = 0$ and $\sin(\beta - \alpha) = 1$. The contribution from the light Higgs h diagram is automatically zero because $S_h = 0$. The contributions from H and A are the same up to the γ^5 factor in the $\phi^0 b\bar{b}$ vertex if they are degenerate. If we look at the diagram more closely, the whole process can be regarded as Wb and $W\bar{b}$ annihilation,

as $2 \rightarrow 2$ processes. It is easy to see from Fig. 2 that for the $Wb \rightarrow H^+b$ subprocess we have three t -channel diagrams with $H_i = h, H, A$ in Fig. 2(a) and one s -channel diagram mediated by the top quark in Fig. 2(b). Similarly, for $W\bar{b} \rightarrow H^+\bar{b}$ subprocess we have three t -channel diagrams with $H_i = h, H, A$ in Fig. 2(c) and one u -channel diagram mediated by the top quark in Fig. 2(d). We have shown in the previous subsection using the effective W approximation that there is strong cancellation among the diagrams, and indeed all four diagrams will exactly cancel one another in the high energy limit. Therefore, if we employ a much lighter CP-odd Higgs boson, which is still allowed by the current data, we expect a strong enhancement to the production cross section of this process. Experimentally, one can use this process to search for the charged Higgs boson and investigate the effects of light CP-odd Higgs boson. Perhaps, a negative search would close out the entire window of light CP-odd Higgs boson.

III. NUMERICAL RESULTS

In this section, we first present some numerical results for the subprocesses $W^+b \rightarrow bH^+$ and $W^+\bar{b} \rightarrow \bar{b}H^+$ for a given value of center-of-mass energy \sqrt{S} and then consider the full process $pp \rightarrow H^+bj$ in the 2HDM of type I (III) and II (IV).

A. The $2 \rightarrow 2$ subprocess in the effective W approximation

We shall limit ourself to the CP conserving case taking $H_1 = h$, $H_2 = H$, and $H_3 = A$. And the couplings of the neutral Higgs bosons to the charged Higgs and W are: $S_h = \cos(\beta - \alpha)$, $S_H = -\sin(\beta - \alpha)$, and $P_A = 1$. Neglecting the contribution from the lightest Higgs boson h as in the decoupling limit $\cos(\beta - \alpha) \rightarrow 0$, we observe that in the high-energy limit the cross section of the subprocess behaves like

$$\sigma(W^+b \rightarrow H^+b) \propto |2c_L + S_H g_H^S + P_A g_A^P|^2 + |S_H g_H^S - P_A g_A^P|^2. \quad (22)$$

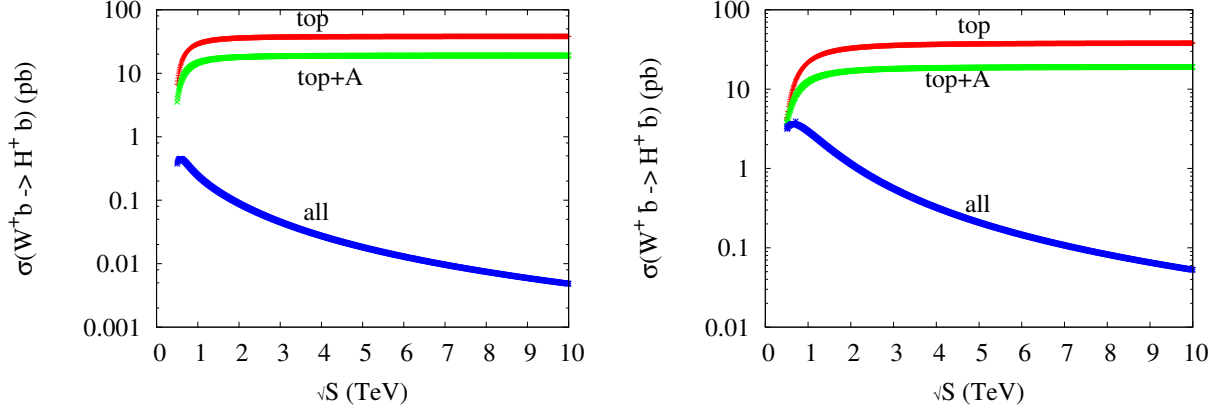


FIG. 3. The cross section as a function of center of mass energy for the subprocess $W^+b \rightarrow H^+b$ (left) and $W^+\bar{b} \rightarrow H^+\bar{b}$ (right) in the MSSM for $\tan\beta = 30$ and $M_A = 400$ GeV.

We note that the cross section suffers a huge cancellation between the top- and Higgs-mediated diagrams. Taking the type II model as an example, we find

$$\begin{aligned}
\sigma(W^+b \rightarrow H^+b)|_{t \text{ only}} &\propto 4 \tan^2 \beta, \\
\sigma(W^+b \rightarrow H^+b)|_{t+H \text{ only}} &= \sigma(W^+b \rightarrow H^+b)|_{t+A \text{ only}} \propto 2 \tan^2 \beta, \\
\sigma(W^+b \rightarrow H^+b)|_{t+H+A} &\propto 0,
\end{aligned} \tag{23}$$

with $c_L = -S_H g_H^S = -P_A g_A^P = \tan\beta$.

Furthermore, independent of the type of 2HDMs we note that for $W^+b \rightarrow H^+b$ (respectively $W^+\bar{b} \rightarrow H^+\bar{b}$) the s -channel (respectively the u -channel) top-exchange diagram interferes destructively with the t -channel Higgs-exchange $W-A$ and $W-H$ fusion diagrams. For demonstration we show in Fig. 3 the cross sections for the subprocess $W^+b \rightarrow H^+b$ (left) and $W^+\bar{b} \rightarrow H^+\bar{b}$ (right) as a function of center of mass energy \sqrt{S} in the MSSM. [‡] We illustrate separately the top diagram alone, the sum of the top and pseudoscalar Higgs exchange diagrams, as well as all four diagrams. Note that “top+A” and “top+H” are extremely close to each other. It is clear from the plot that the dominant contribution is coming from the top diagram. It is also visible from the plot that the interference between s -channel top diagram and $W-A$ fusion is destructive. The top contribution is reduced by a factor of 2 by the $W-A$ fusion diagram and same destructive interference takes place with $W-H$ fusion diagram. We

[‡] Though we are working in the framework of 2HDMs, M_{H^+} , M_H , and M_A are very close to one another in the MSSM that will suit our purpose here.

only show the sum of the top diagram and W - A fusion diagram in the figure, that of the top and W - H fusion diagrams is almost the same. As expected from Eq. (23), in the case of $W^+b \rightarrow H^+b$, after inclusion of all diagrams the total cross section drops by more than 3 orders of magnitude at large \sqrt{S} , as shown on the left panel of Fig. 3. This in fact is due to the strong destructive interference of top diagram with the W - A and W - H fusion diagrams. Similarly, on the right panel in Fig. 3 we illustrate the cross section for $W^+\bar{b} \rightarrow H^+\bar{b}$ as a function of \sqrt{S} . Again, as expected we can see destructive interference between u -channel top diagram and t -channel W - A and W - H fusion diagrams. We stress that the destructive interference in the \bar{b} -initiated process is less severe than the b -initiated one, such that the total cross section for $W^+\bar{b} \rightarrow H^+\bar{b}$ is about one order of magnitude larger than that for $W^+b \rightarrow H^+b$, even though the “top-only” cross section for the \bar{b} -initiated process starts out smaller than the b -initiated one. This is because the u -channel top-quark propagator has an angular dependence such that the denominator of the propagator factor itself does not always attain a high enough energy to enable a complete cancellation.

B. For full process $pp \rightarrow H^\pm bj$

In the previous subsection we have shown analytically and illustrated numerically the cancellation in the subprocesses $W^+b \rightarrow bH^+$ and $W^+\bar{b} \rightarrow H^+\bar{b}$ between the top diagram and W - A and W - H fusion diagrams using the effective W approximation. In Fig. 4, we show the cross sections for the full $2 \rightarrow 3$ processes $qb \rightarrow q'H^+b$ (upper panels), $q\bar{b} \rightarrow q'H^+\bar{b}$ (middle panels), and their sum (lower panels) as functions of $\tan\beta$ (left panels) and $M_{H^+} = M_A = M_H$ (right panels), including the charged-conjugate channels and after folding with the parton distribution functions. Again, we separately show the contributions from the top diagram only, the top plus W - A fusion diagrams, the top plus W - H fusion diagrams, and all diagrams. We have assumed that we are in the decoupling limit $\sin\alpha = -\cos\beta$ and taking a spectrum of degenerate Higgs bosons $M_{H^\pm} = M_H = M_A$ as in the MSSM and the lightest CP-even Higgs boson h is the observed one with $m_h = 125.09$ GeV. Thus, the diagram with h proportional to $\cos(\beta - \alpha)$ does not contribute while the amplitudes associated with the A and H diagrams are the same up to a factor of γ^5 in the $Ab\bar{b}$ and $Hb\bar{b}$ vertex. Also, we can see that in the b -initiated subprocess (upper panels) the “top+ A ” curve completely overlaps with “top+ H ” curves but not exactly in the \bar{b} -initiated one (middle panels).

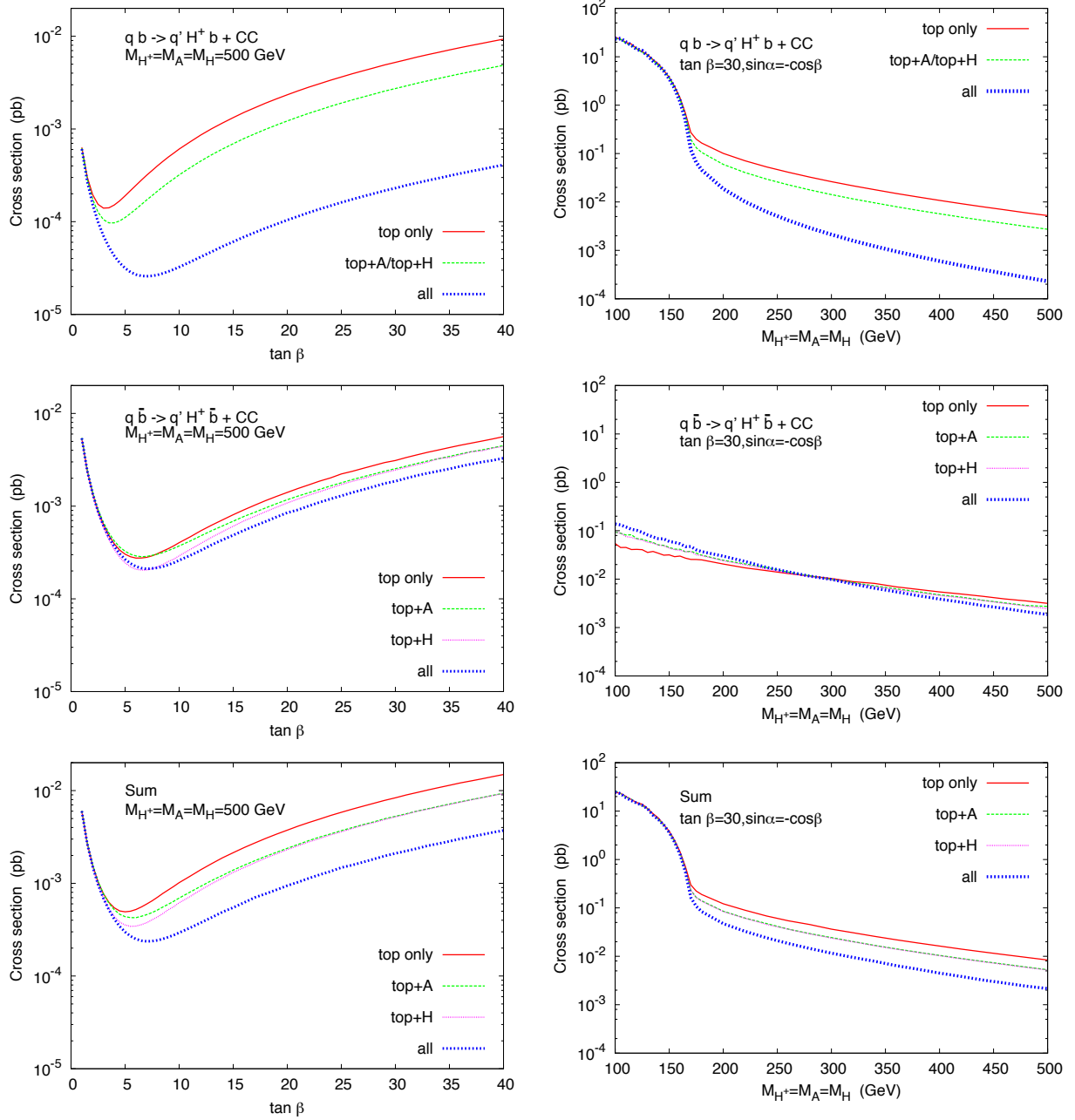


FIG. 4. The $pp \rightarrow H^\pm b j$ cross sections in the 2HDM type II as functions of $\tan \beta$ (left panels) and charged Higgs mass (right panels) at LHC-14. The upper panels are the b initiated process, the middle panels are \bar{b} initiated process while the lower panel are the sum of b and \bar{b} . The charged conjugate panels are included in the plots. All panels are for the decoupling limit $\sin \alpha = -\cos \beta$.

The upper panels in Fig. 4 illustrate a very strong cancellation between the top diagram, and W - A and W - H fusion diagrams. Note the charged-conjugate channels $\bar{q}\bar{b} \rightarrow \bar{q}'H^-\bar{b}$ are included in it. On the other hand, the middle panels show a less severe cancellation between

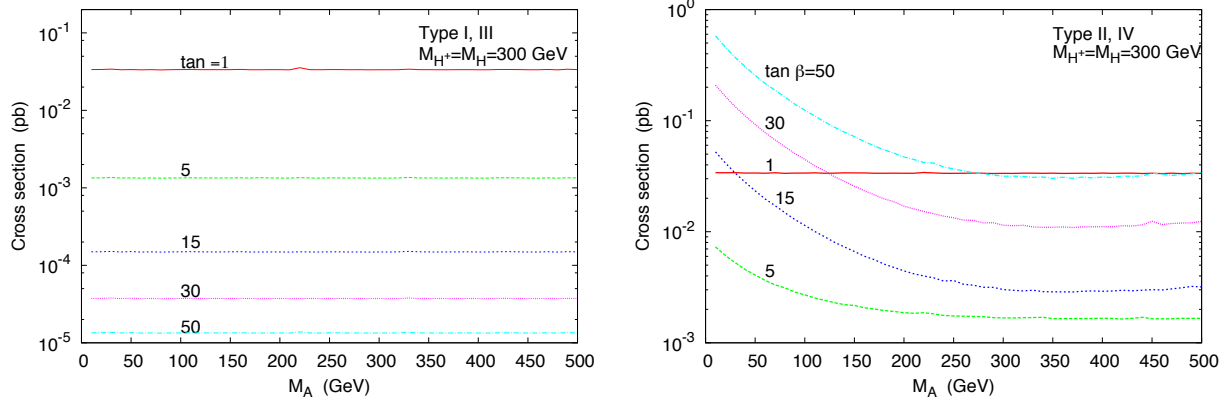


FIG. 5. The $pp \rightarrow H^\pm bj$ cross sections at LHC-14 as a function of M_A in the 2HDM type I and III (left), and II and IV (right) for several values of $\tan \beta$. We have taken $M_{H^\pm} = M_H = 300$ GeV.

the top diagram, and W - A and W - H fusion diagrams where the charged-conjugate channels $\bar{q}b \rightarrow \bar{q}'H^-b$ are also included in it. Therefore, we still see that a strong cancellation occurs for the full process $pp \rightarrow H^\pm bj$ at the LHC-14, shown in the lower panels.

It is clear from the left panels that the cross sections are enhanced for both small $\tan \beta \approx 1$ and large $\tan \beta$, the latter of which is associated with enhanced bottom Yukawa couplings. A dip indeed occurs around $\tan \beta \approx 6$ in the $\tan \beta$ plots, which corresponds to where the top and bottom Yukawa couplings become similar $m_b \tan \beta \approx m_t / \tan \beta$. We stress that our results are in good agreement with Ref. [9].

As shown on the right panels, we emphasize that for $M_{H^\pm} \leq m_t - m_b$ the top quark can be produced on-shell as in single-top production and then decays into bH^+ . Therefore, in the range of $M_{H^\pm} \leq m_t - m_b$ the top-exchange diagram completely dominates over other diagrams. On the other hand, for $M_{H^\pm} > m_t - m_b$ the top quark is off-shell, and thus other diagrams also make significant contributions. Note that in the \bar{b} -initiated process $q\bar{b} \rightarrow q'H^+\bar{b}$ the top quark is never produced on-shell.

It is well known that in the MSSM and for $M_A \geq 200$ GeV all the heavy Higgs bosons become degenerate $M_H = M_A = M_{H^\pm}$ and $\cos(\beta - \alpha) \rightarrow 0$. In general 2HDMs all Higgs boson masses are independent parameters. One can then identify the lightest CP-even with the observed 125 GeV Higgs boson and take the others M_H , M_A and M_{H^\pm} as free parameters. In Fig. 5, we show the total cross sections as a function of the CP-odd Higgs mass for a few values of $\tan \beta = 1 - 50$ and $M_H = M_{H^\pm} = 300$ GeV in 2HDMs types I and III (left

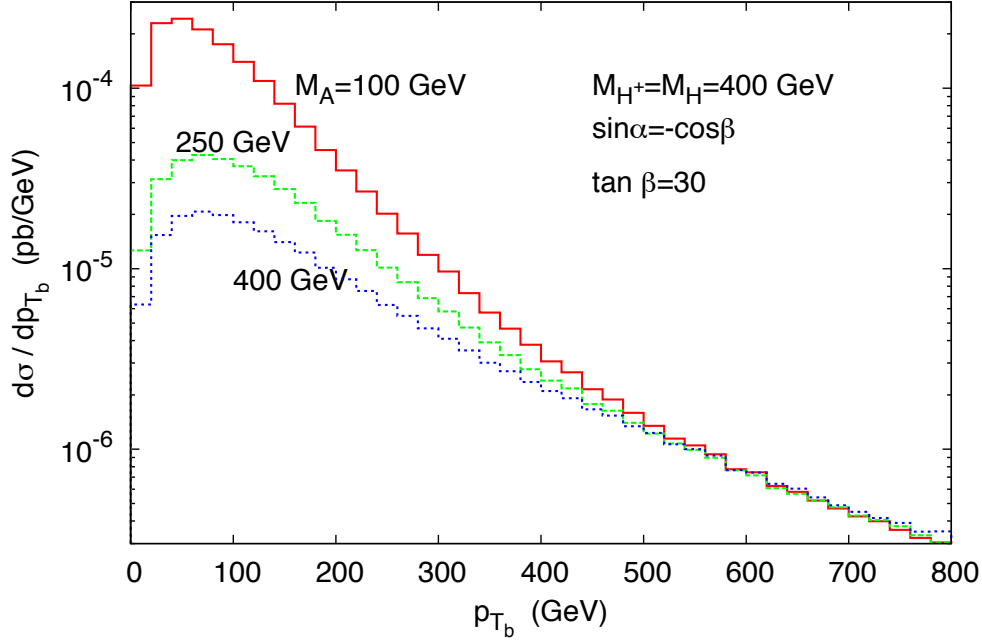


FIG. 6. The transverse momentum p_{T_b} distribution for $pp \rightarrow H^\pm bj$ in 2HDM type II and IV at the LHC-14 for $M_A = 100, 250, 400$ GeV. We have taken the decoupling limit $\sin \alpha = -\cos \beta$, $\tan \beta = 30$, and $M_{H^\pm} = M_H = 400$ GeV.

panel) and types II and IV (right panels). For the values of the couplings in production cross sections, we refer to Table II. In types I and III, the cross sections are insensitive to the CP-odd Higgs mass and they are suppressed by $1/\tan^2 \beta$ with increasing $\tan \beta$. The largest value of the cross section is obtained at $\tan \beta = 1$ and is of the order 27 fb. In types II and IV, one can see some sensitivity to the CP-odd Higgs mass. For $M_A \leq 250$ GeV, the cross section increases for lighter CP-odd Higgs mass and becomes almost constant for $M_A \geq 250$ GeV. The enhancement of the cross section for $M_A \leq 250$ GeV is amplified with large values of $\tan \beta$. For $M_A = 100$ GeV and $\tan \beta = 30$ one can reach a cross section of the order of 40 fb.

In Fig. 6, we plot the p_{T_b} distribution of the b quark in the decoupling limit and for $M_{H^\pm} = M_H = 400$ GeV and $\tan \beta = 30$ for several values of $M_A = 100, 250$ and 400 GeV. As one can see from the plot, the distribution is enhanced for light $M_A = 100$ GeV and for $p_{T_b} \leq 200$ GeV. The transverse momentum of the b quark is then a useful variable to separate the contributions between the top diagram and the W - A fusion diagram. One can

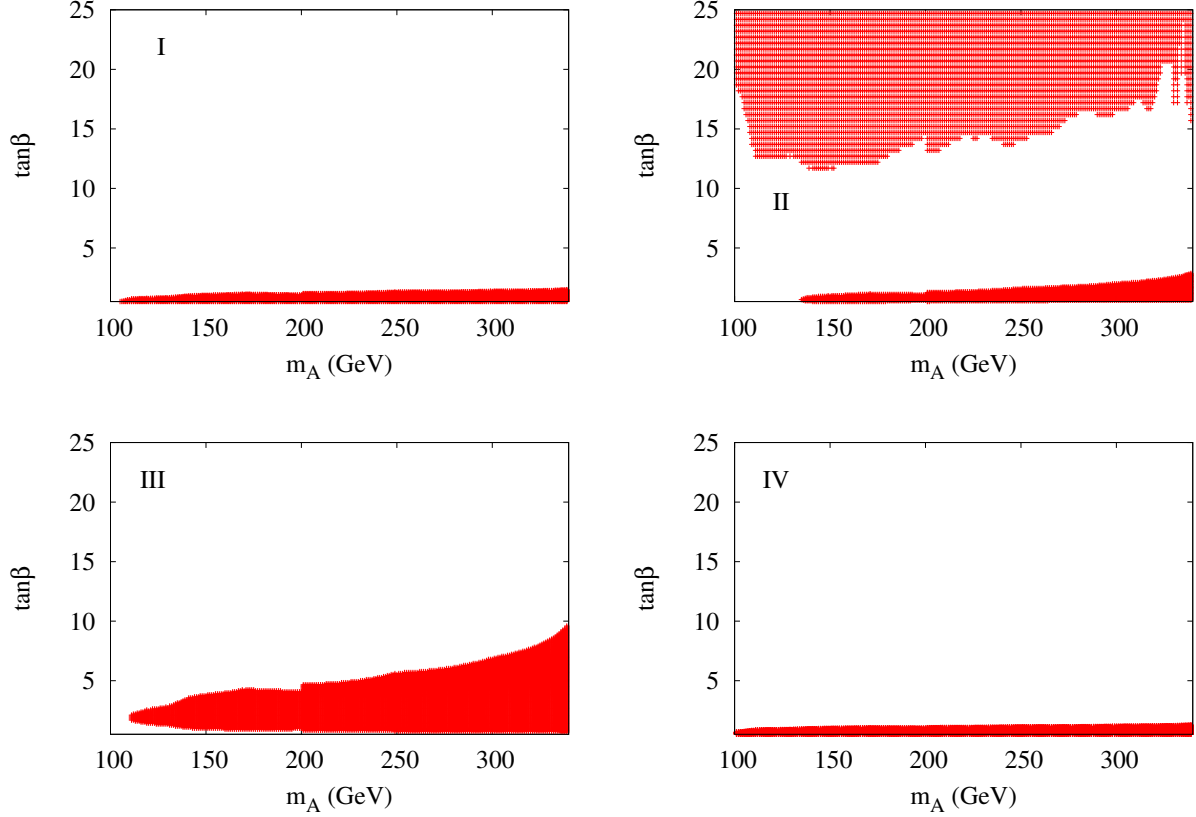


FIG. 7. Exclusion plots in the plane of $(M_A, \tan \beta)$ for the 2HDMs type I, II, III and IV, using the ATLAS data for $gg \rightarrow A \rightarrow \tau^+ \tau^-$. The excluded region is shown in red while the rest is allowed.

require $p_{T_b} < 200$ GeV to suppress the top-exchange contribution.

C. Large $\tan \beta$ and LHC $pp \rightarrow \Phi \rightarrow \tau^+ \tau^-$ data

At the LHC with 7 and 8 TeV, searches for the Higgs bosons Φ that decay into tau pairs, which in turn decay into those final states with one or two light leptons, have been performed [24, 25] for Higgs mass in the range [100, 900] GeV. Both ATLAS and CMS have some exclusion limits given as $\sigma(gg \rightarrow \Phi) \times B(\Phi \rightarrow \tau^+ \tau^-)$ as a function of the Higgs mass m_Φ . These limits can be interpreted in the 2HDMs if we take the Higgs state Φ as one of the neutral Higgs bosons of the 2HDMs: $\Phi = h$ and/or H, A . In fact if h mimics the SM Higgs boson, $\sigma(gg \rightarrow h) \times B(h \rightarrow \tau^+ \tau^-)$ will not have any enhancement factor such as $\tan \beta$. Since we have observed that in order to enhance $pp \rightarrow bH^+ j$ cross sections one needs both non-degenerate A and H and also large $\tan \beta$, here we attempt to find what

would be the largest possible value for $\tan\beta$ such that it is still consistent with $\tau^+\tau^-$ data for $100 \leq M_A \leq 340$ GeV and assuming that the heavy CP-even Higgs boson is rather heavy. A similar study with the 7 TeV data had been done in [26] for 2HDM. Because of CP invariance the CP-odd Higgs boson A does not couple to WW or ZZ , and the partial decay widths into loop mediated gg , $\gamma\gamma$, and γZ channels are highly suppressed. The decay channel $A \rightarrow hZ$, which is proportional to $\cos(\beta - \alpha)$, will also be severely suppressed if we assume that $\beta - \alpha$ is close to the decoupling limit. Therefore, the CP-odd Higgs boson predominantly decays into fermion pairs: $q\bar{q}$, $q = b, s, d, c, u$ and l^+l^- $l = \tau, \mu, e$.

In 2HDM-I and -IV, the coupling $A\tau^+\tau^-$ is proportional to $1/\tan\beta$ while in 2HDM-II and -III it is proportional to $\tan\beta$. On the other hand, from Table I the coupling of $A b\bar{b}$ is proportional to $\tan\beta$ in 2HDM-II and -IV but $1/\tan\beta$ in 2HDM-I and -III. Thus, it is clear that in 2HDM-I (resp. II) both the production rate $gg \rightarrow A$ and the decay $A \rightarrow \tau^+\tau^-$ are suppressed (resp. enhanced) for large $\tan\beta$. We then expect a strong exclusion for large $\tan\beta$ in type II but not in type I. In all four 2HDM types we expect some enhancement for small $0.5 \leq \tan\beta \leq 1$ because $At\bar{t}$ is proportional to $m_t/\tan\beta$.

For a given CP-odd Higgs mass M_A and $\tan\beta$, the cross section of $gg \rightarrow A$, which only depends on these 2 parameters, is computed with help of SUSHI public code [27]. In the decoupling limit $A \rightarrow Zh$ is vanishing, and if $A \rightarrow \{W^\pm H^\mp, ZH, t\bar{t}\}$ are closed, the branching ratio of $A \rightarrow \tau^+\tau^-$ depends on $\tan\beta$ and M_A only, and there is no $\sin\alpha$ dependence. Therefore, the cross section $gg \rightarrow A \rightarrow \tau^+\tau^-$ will depend only on $\tan\beta$ and M_A . Hence, our exclusion from $\tau^+\tau^-$ data can be given in the plane of $(M_A, \tan\beta)$. After computing the cross section $gg \rightarrow A$ times the branching fraction of $A \rightarrow \tau^+\tau^-$, we compare our theoretical predictions with the ATLAS data [24]. Note that the ATLAS data were given for $M_A = 90, 100, \dots, 340$ GeV with steps of 10 GeV or even larger in some cases. Therefore, we have used linear interpolations for M_A values in-between the data.

We draw in Fig. 7 the exclusion region in $(M_A, \tan\beta)$ plane for 2HDMs type I, II, III, and IV, where M_A is in the range $[100, 340]$ GeV and $0.5 \leq \tan\beta \leq 50$. In 2HDM types I and IV, there is no exclusion for $\tan\beta \geq 1.5$. The reason is that in type I, the production rate of $gg \rightarrow A$ and decay of $A \rightarrow \tau^+\tau^-$ are both suppressed by $1/\tan\beta$. Whereas in 2HDM type IV, the production rate is enhanced by the bottom Yukawa for large $\tan\beta$ but the decay $A \rightarrow \tau^+\tau^-$ is suppressed by $1/\tan\beta$ which cancels the bottom enhancement in the production, which then gives no exclusion for large $\tan\beta$. In 2HDM type III, similar to type

I the production rate is suppressed by $1/\tan\beta$. However, the branching fractions of $A \rightarrow q\bar{q}$ are suppressed by $1/\tan\beta$ while $B(A \rightarrow \tau^+\tau^-)$ is enhanced for large $\tan\beta$. For this reason the exclusion in type III is somewhat stronger than that in type I. There is no exclusion for $\tan\beta \geq 9.5$ (resp. $\tan\beta \geq 2$) for $M_A \approx 340$ GeV (resp. for $M_A \approx 112$ GeV). On the other hand, the 2HDM-II receives both enhancement at large $\tan\beta$ for the production rate $gg \rightarrow A$ and the $B(A \rightarrow \tau^+\tau^-)$. Thus, this gives a strong exclusion for $\tan\beta \geq 22$ for all $M_A \in [100, 340]$ GeV. The low $\tan\beta \leq 3$ region (resp. $\tan\beta \leq 1$) is also excluded for $M_A = 340$ GeV (resp. $M_A = 150$ GeV).

IV. BEYOND TWO-HIGGS-DOUBLET MODELS

Taking one of the 2HDMs as a low-energy reference model, the relevant interactions may be parameterized as

$$\begin{aligned}\mathcal{L}_{H_i\bar{b}b} &= -\frac{gm_b}{2m_W} \bar{b} (\xi_i^S g_i^S + i \xi_i^P g_i^P \gamma_5) b H_i, \\ \mathcal{L}_{H^\pm tb} &= +\frac{gm_b}{\sqrt{2}m_W} \bar{b} (\xi_L c_L P_L + \xi_R c_R P_R) t H^\pm + \text{h.c.}, \\ \mathcal{L}_{H_i H^\pm W^\pm} &= -\frac{g}{2} (\xi_S S_i + i \xi_P P_i) \left[H^\pm \left(i \overleftrightarrow{\partial}_\mu \right) H_i \right] W^{\pm\mu} + \text{h.c.}\end{aligned}\quad (24)$$

In the MSSM, for example, including the $\tan\beta$ -enhanced SUSY threshold corrections to the down-type Yukawa couplings, we have

$$\xi_i^S = \xi_i^P = \xi_L = \frac{1}{1 + \kappa_b \tan\beta}, \quad \xi_R = \xi_S = \xi_P = 1, \quad (25)$$

with [28]

$$\kappa_b = \epsilon_g + \epsilon_H,$$

where ϵ_g and ϵ_H are the contributions from the sbottom-gluino exchange diagram and from stop-Higgsino diagram, respectively. Their explicit expressions are

$$\epsilon_g = \frac{2\alpha_s}{3\pi} M_3^* \mu^* I(m_{\tilde{b}_1}^2, m_{\tilde{b}_2}^2, |M_3|^2), \quad \epsilon_H = \frac{|h_t|^2}{16\pi^2} A_t^* \mu^* I(m_{\tilde{t}_1}^2, m_{\tilde{t}_2}^2, |\mu|^2),$$

where M_3 is the gluino mass parameter, h_t and A_t are the top-quark Yukawa and trilinear couplings, respectively.

Without loss of generality we choose the 2HDM type II as the reference model, and show the change in production cross sections with the variations in the couplings $\xi_i^{S,P}$ and ξ_L .

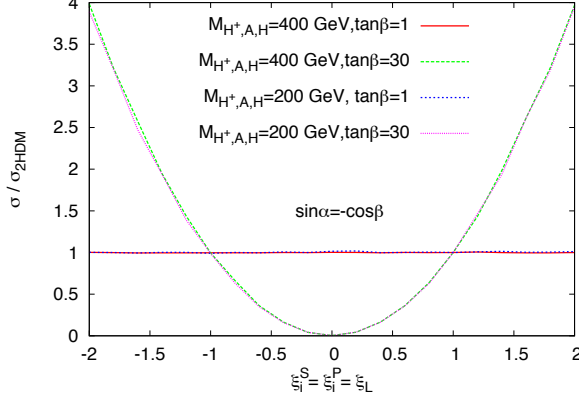


FIG. 8. Ratios of cross sections for varying $\xi_i^S = \xi_i^P = \xi_L$ to the cross section at the 2HDM type II value ($\xi_i^S = \xi_i^P = \xi_L = 1$).

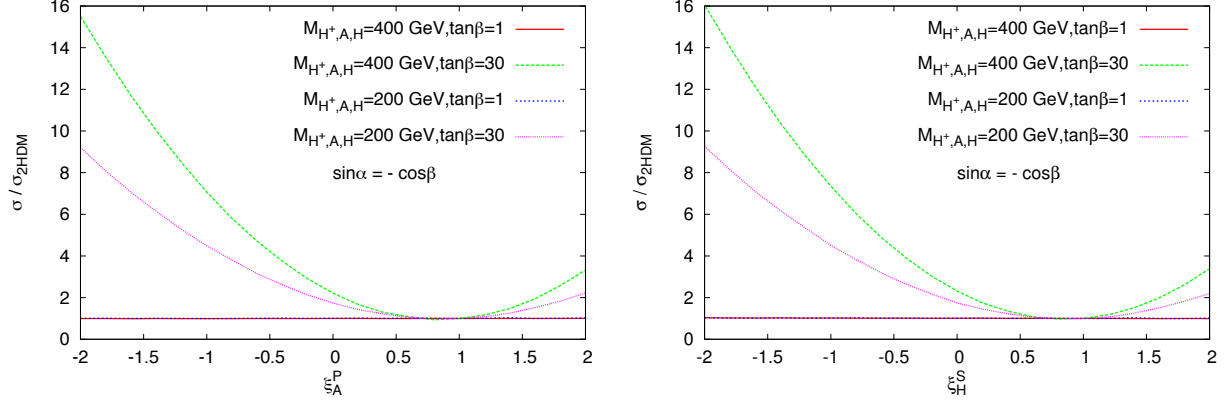


FIG. 9. Ratios of cross section with varying ξ_A^P (left panel) or ξ_H^S (right panel) to the cross section at the 2HDM value (i.e. $\xi_A^P = 1$ or $\xi_H^S = 1$ respectively) by keeping all other parameters at their 2HDM type II values.

We used Eq. (25) as the guidance. We first show the ratio of the cross sections for varying $\xi_i^S = \xi_i^P = \xi_L$ between -2 and $+2$ to the cross section at the 2HDM type II values, i.e., $\xi_i^S = \xi_i^P = \xi_L = 1$ in Fig. 8, for $\tan\beta = 1, 30$. The $\tan\beta = 1$ curves show almost no sensitivity to $\xi_i^S = \xi_i^P = \xi_L$ because the process is dominated by the top-Yukawa term. On the other hand, the $\tan\beta = 30$ curves are dominated by the bottom-Yukawa term. It is obvious that the ratio is close to zero for $\xi_i^S = \xi_i^P = \xi_L = 0$, and is one for $\xi_i^S = \xi_i^P = \xi_L = 1$. The ratio grows as the square of the couplings around 0 to almost 4 at $\xi_i^S = \xi_i^P = \xi_L = \pm 2$.

If for some higher scale dynamics such that ξ_i^S and ξ_i^P do not change in the same manner,

we show the effects on the cross sections in Fig. 9. On the left panel, we show the ratio of cross sections with varying ξ_A^P between -2 and $+2$ to the cross section at the 2HDM value (i.e. $\xi_A^P = 1$) by keeping all other parameters at their 2HDM type II values. Again, the sensitivity at $\tan\beta = 1$ is negligible, while it becomes quite nontrivial for large $\tan\beta = 30$. As we have shown in Sec. III that the W - A diagram interferes destructively with the top diagram, we can now turn the destructive interference into constructive one by reversing the sign of ξ_A^P . Furthermore, when ξ_A^P is negative the second term in Eq. (22) would not vanish. It is then very clear that the ratio becomes quite large at negative ξ_A^P . At $\xi_A^P = 0$, the ratio is already larger than 1 because no interference comes from the W - A diagram. Similar behavior occurs for ξ_H^S as shown on the right panel in Fig. 9. The ratios that ξ_H^S can attain are very similar to those of ξ_A^P .

V. CONCLUSIONS

We have performed the study of b - and \bar{b} -initiated processes of $pp \rightarrow jH^\pm b/\bar{b}$ in the 2HDM framework at the LHC-14 in the decoupling limit ($\sin\alpha = -\cos\beta$), which is favored by the current Higgs data. We have identified strong cancellations between the top diagram and the W - H_i ($H_i = h, H, A$) diagrams which rendered the process very suppressed. The cancellation is indeed the strongest when the A and H are degenerate and in the decoupling limit. We pointed out that if the pseudoscalar Higgs boson A is much lighter than the CP-even Higgs boson H , the cross section of charged-Higgs production can be substantially enhanced, because the cancellation is no longer complete. We have explicitly obtained the exclusion in parameter space of $(M_A, \tan\beta)$ for 2HDM types I to IV based on the LHC data on $\sigma(g \rightarrow \Phi) \times B(\Phi \rightarrow \tau^+\tau^-)$. In the allowed parameter space, the size of production cross section can be as large as $\mathcal{O}(50)$ fb for $M_A = 100$ GeV and $\tan\beta = 30$ for types II and IV. This is the main result of the work.

We offer the following comments on the findings of this work as follows.

1. The b -initiated process for production of H^+ in $qb \rightarrow qH^+b$ suffers from a very strong cancellation between the top diagram and the W - H_i diagrams. However, the \bar{b} -initiated process for production of H^+ in $q\bar{b} \rightarrow qH^+\bar{b}$ suffers a less severe cancellation, mainly because of the u -channel top-exchange instead of s -channel.

2. The strong cancellation is dictated by the absence of the unitarity-breaking terms and we find the sum rules expressed by the relevant Higgs couplings, see Eq. (18).
3. For $M_{H^\pm} \leq m_t - m_b$ the top diagram completely dominates as the top quark is produced on-shell as like that in single-top production. However, when $M_{H^\pm} > m_t - m_b$ the W - H_i fusion diagrams also contribute.
4. In the future study, we shall make use of the special kinematics, e.g, the p_{T_b} distribution, to discriminate between the top and the W - H_i fusion diagrams. The goal is to isolate the effect of light pseudoscalar Higgs boson, which is still allowed by the current data.
5. Current LHC data on $\sigma(gg \rightarrow \Phi) \times B(\Phi \rightarrow \tau^+\tau^-)$ constrains the parameters of the 2HDMs. We found that the data constrains the most on type II because both the production process and the decay are $\tan\beta$ enhanced. Yet, there are sizable allowed parameter space between $\tan\beta = 3$ and 22. The second most constrained is type III because the production rate is suppressed by $1/\tan\beta$ but the decay is enhanced by $\tan\beta$. Types I and IV have the most available parameter space.
6. The process $pp \rightarrow jH^\pm b/\bar{b}$ that we consider in this work would be more interesting for type II and IV because of larger cross sections. Especially type IV has the least restriction from the current LHC data on $\sigma(gg \rightarrow \Phi) \times B(\Phi \rightarrow \tau^+\tau^-)$, and it can allow cross sections as large as $O(100 - 300)$ fb for $\tan\beta = 30 - 50$ and $M_A = 50 - 100$ GeV.
7. When the 2HDM is a low-energy limit of some ultraviolet (UV) models, the integrity of the Yukawa couplings may change. For example, in the MSSM the SUSY particles can largely change the bottom-Yukawa couplings with strong and weak interactions. Varying the bottom Yukawa coupling of either A or H gives non-trivial behavior for the production cross sections.

ACKNOWLEDGMENT

We thanks Marco O. P Sampaio for providing us with CP-odd cross sections. K.C. was supported by the MoST of Taiwan under Grants number 102-2112-M-007-015-MY3.

J.S.L. was supported by the National Research Foundation of Korea (NRF) grant (No. 2013R1A2A2A01015406) and by the Chonnam National University, 2012. A.A would like to thank NCTS for warm hospitality where part of this work has been done.

-
- [1] G. Aad *et al.* [ATLAS Collaboration], Phys. Lett. B **716** (2012) 1 [arXiv:1207.7214 [hep-ex]];
 - [2] S. Chatrchyan *et al.* [CMS Collaboration], Phys. Lett. B **716** (2012) 30 [arXiv:1207.7235 [hep-ex]].
 - [3] G. Aad *et al.* [ATLAS and CMS Collaborations], Phys. Rev. Lett. **114** (2015) 191803 [arXiv:1503.07589 [hep-ex]].
 - [4] K. Cheung, J. S. Lee and P. Y. Tseng, JHEP **1305** (2013) 134 [arXiv:1302.3794 [hep-ph]].
 - [5] K. Cheung, J. S. Lee and P. Y. Tseng, Phys. Rev. D **90**, 095009 (2014) [arXiv:1407.8236 [hep-ph]].
 - [6] V. D. Barger, R. J. N. Phillips and D. P. Roy, Phys. Lett. B **324**, 236 (1994); J. F. Gunion, H. E. Haber, F. E. Paige, W. K. Tung and S. S. D. Willenbrock, Nucl. Phys. B **294**, 621 (1987). R. M. Barnett, H. E. Haber and D. E. Soper, Nucl. Phys. B **306**, 697 (1988). J. L. Diaz-Cruz and O. A. Sampayo, Phys. Rev. D **50**, 6820 (1994). F. Borzumati, J. L. Kneur and N. Polonsky, Phys. Rev. D **60**, 115011 (1999) [hep-ph/9905443].
 - [7] D. A. Dicus, J. L. Hewett, C. Kao and T. G. Rizzo, Phys. Rev. D **40**, 787 (1989). A. A. Barrientos Bendezu and B. A. Kniehl, Phys. Rev. D **59**, 015009 (1999); A. A. Barrientos Bendezu and B. A. Kniehl, Phys. Rev. D **63**, 015009 (2001); W. Hollik and S. h. Zhu, Phys. Rev. D **65**, 075015 (2002); O. Brein, W. Hollik and S. Kanemura, Phys. Rev. D **63**, 095001 (2001).
 - [8] Q. H. Cao, S. Kanemura and C. P. Yuan, Phys. Rev. D **69**, 075008 (2004).
 - [9] S. Moretti and K. Odagiri, Phys. Rev. D **55**, 5627 (1997).
 - [10] A. C. Bawa, C. S. Kim and A. D. Martin, Z. Phys. C **47**, 75 (1990). A. A. Barrientos Bendezu and B. A. Kniehl, Nucl. Phys. B **568**, 305 (2000); A. Krause, T. Plehn, M. Spira and P. M. Zerwas, Nucl. Phys. B **519**, 85 (1998).
 - [11] S. Dittmaier, G. Hiller, T. Plehn and M. Spannowsky, Phys. Rev. D **77**, 115001 (2008) [arXiv:0708.0940 [hep-ph]].
 - [12] G. Aad *et al.* [ATLAS Collaboration], JHEP **1503**, 088 (2015) [arXiv:1412.6663 [hep-ex]].

- [13] V. Khachatryan *et al.* [CMS Collaboration], arXiv:1508.07774 [hep-ex]. S. Chatrchyan *et al.* [CMS Collaboration], JHEP **1207**, 143 (2012) [arXiv:1205.5736 [hep-ex]]. CMS Collaboration [CMS Collaboration], CMS-PAS-HIG-14-020.
- [14] V. D. Barger, R. J. N. Phillips and D. P. Roy, Phys. Lett. B **324**, 236 (1994); D. J. Miller, S. Moretti, D. P. Roy and W. J. Stirling, Phys. Rev. D **61**, 055011 (2000); S. Moretti and D. P. Roy, Phys. Lett. B **470**, 209 (1999);
- [15] K. Odagiri, arXiv:hep-ph/9901432; S. Raychaudhuri and D. P. Roy, Phys. Rev. D **53**, 4902 (1996).
- [16] S. Yang and Q. S. Yan, JHEP **1202**, 074 (2012) [arXiv:1111.4530 [hep-ph]].
- [17] M. Drees, M. Guchait and D. P. Roy, Phys. Lett. B **471**, 39 (1999); S. Moretti, Phys. Lett. B **481**, 49 (2000).
- [18] K. Cheung and D. K. Ghosh, JHEP **0211**, 048 (2002) [hep-ph/0208254]; C. W. Chiang and K. Tsumura, JHEP **1504**, 113 (2015) [arXiv:1501.04257 [hep-ph]].
- [19] G. C. Branco, P. M. Ferreira, L. Lavoura, M. N. Rebelo, M. Sher and J. P. Silva, Phys. Rept. **516**, 1 (2012) [arXiv:1106.0034 [hep-ph]].
- [20] K. Cheung, J. S. Lee and P. Y. Tseng, “Higgscision in the Two-Higgs Doublet Models,” JHEP **1401** (2014) 085 [arXiv:1310.3937 [hep-ph]].
- [21] S. Davidson and H. E. Haber, “Basis-independent methods for the two-Higgs-doublet model,” Phys. Rev. D **72** (2005) 035004 [Erratum-ibid. D **72** (2005) 099902] [hep-ph/0504050].
- [22] S. L. Glashow and S. Weinberg, “Natural Conservation Laws for Neutral Currents,” Phys. Rev. D **15** (1977) 1958.
- [23] J. F. Gunion and H. E. Haber, Phys. Rev. D **67**, 075019 (2003) [hep-ph/0207010].
- [24] G. Aad *et al.* [ATLAS Collaboration], “Search for neutral Higgs bosons of the minimal supersymmetric standard model in pp collisions at $\sqrt{s} = 8$ TeV with the ATLAS detector,” JHEP **1411**, 056 (2014) [arXiv:1409.6064 [hep-ex]].
- [25] CMS Collaboration [CMS Collaboration], “Higgs to tau tau (MSSM),” CMS-PAS-HIG-13-021.
- [26] A. Arhrib, C. W. Chiang, D. K. Ghosh and R. Santos, Phys. Rev. D **85**, 115003 (2012) [arXiv:1112.5527 [hep-ph]].
- [27] R. V. Harlander, S. Liebler and H. Mantler, Comput. Phys. Commun. **184**, 1605 (2013) [arXiv:1212.3249 [hep-ph]].
- [28] F. Borzumati, J. S. Lee, W. Y. Song, Phys. Lett. **B595** (2004) 347, [hep-ph/0401024].